ACS APPLIED MATERIALS & INTERFACES

Research Article

www.acsami.org

Silicon Nanowires/Reduced Graphene Oxide Composites for Enhanced Photoelectrochemical Properties

Zhipeng Huang,*[,†] Peng Zhong,[†] Chifang Wang,[†] Xuanxiong Zhang,[‡] and Chi Zhang*[,†]

[†]Functional Molecular Materials Research Centre, Scientific Research Academy, Jiangsu University, Zhenjiang 212013, P. R. China

[‡]Shanghai Key Laboratory of Modern Optical System, School of Optical-Electrical and Computer Engineering, University of Shanghai for Science and Technology, Shanghai 200093, P. R. China

Supporting Information

ABSTRACT: The top of silicon nanowires (SiNWs) arrays was coated with reduced graphene oxide (rGO) by the facile spin-coating method. The resulting SiNWs/rGO composite exhibits enhanced photoelectrochemical properties, with short-circuit photocurrent density more than 4 times higher than that of the pristine SiNWs and more than 600 times higher than that of planar Si/rGO composite. The trapping and recombination of photogenerated carriers at the surface state of SiNWs were reduced after the application of rGO. The results of electrochemical impedance spectroscopy measurements suggest that the reduction of trapping and recombination of photogenerated carriers as well as remarkably enhancement of photoelectrochemical properties can be attributed to the low charge transfer resistance at the SiNWs−rGO interface and rGO−electrolyte interface. The method and results shown here indicate a convenient and applicable approach to further exploitation of high activity materials for photoelectrochemical applications.

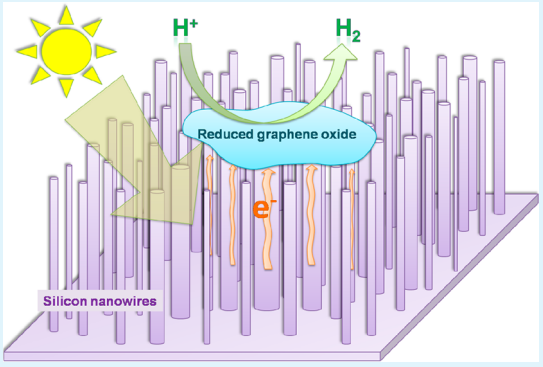

KEYWORDS: *silicon, nanowires, graphene, photocatalyst, photoelectrochemisty*

INTRODUCTION

As a kind of earth abundant semiconductor, silicon (Si) gains extensive attention in the field of light harvesting because Si possesses a narrow band gap enabling the absorption of the solar radiation energy ranging from ultraviolet to visible light. Meanwhile, one-dimensional semiconductor nanostructures exhibit promising application potential in the field of photovoltaics because of their remarkably improved optical absorption or/and charge collection ability in comparison with the bulk materials and zero-dimensional nanostructures.[1] As a result, solar light harvesting using Si nanowires (SiNWs) and Si microwires (SiMWs) gains increasing importance.[2−8] However, in the photovoltaics application involving chemical processes (e.g., photoelectrochemical hydrogen production and photoelectrochemical solar cell), the performances of Si-based devices are usually limited by slow kinetics at the Si−electrolyte interface. The introduction of noble metal particles (e.g., Pt) to the surface of planar Si, SiNWs, and SiMWs has been proved to be an efficient approach for the improvement of their photoelectrochemical performance.[3,9−12] The use of expensive and earth rare noble metal, however, limits the wide application of this approach in photoelectrochemical light harvesting, and the low-cost strategy affording the improvement of photoelectrochemical performance of Si remains a big challenge. Various approaches have been developed to improve the intrinsic low photoelectrochemical performance of SiNWs or SiMWs, including surface modification with low-cost and earth abundant electrocatalyst (e.g., Ni−Mo,[13] Mo_3S_4 cluster,[6] and MoS_2[14]) and surface energy band engineering (e.g., n^+ doping[11] and SiNWs/ZnO nanowire heterostructures[15]).

As new-emerging two-dimensional material, graphene[16] has attracted much attention in numerous applications including transparent conducting, dye sensitized solar cell, super capacitance, and etc. because of its stability, high surface area, optical transparency, and high carrier mobility.[17,18] The composites of reduced graphene oxide (rGO) and semiconductor photocatalysts (e.g., TiO_2,[19] CdS,[20] and $Zn_xCd_{1-x}S$,[21] $BiVO_4$[22]) exhibit excellent photoelectrochemical water splitting capability, and such excellent performance has been attributed to the fast charge separation in photocatalyst and fast interfacial charge transfer at the photoelectrode−electrolyte interface in the presence of rGO. Graphene has also been utilized to construct a Schottky junction on the surface of planar Si[23,24] and SiNWs,[25,26] enabling light harvesting from Si/graphene composite. On the other hand, Si/graphene composites can be used as improved anode materials for lithium ion batteries.[27−30]

Herein we report the convenient fabrication of SiNWs/rGO composites for enhanced photoelectrochemical properties. SiNWs and rGO were fabricated, respectively, by low-cost metal-assisted chemical etching (MACE)[31] and an improved

Received: November 19, 2012
Accepted: February 22, 2013
Published: February 22, 2013

dx.doi.org/10.1021/am3027458 | ACS Appl. Mater. Interfaces 2013, 5, 1961−1966

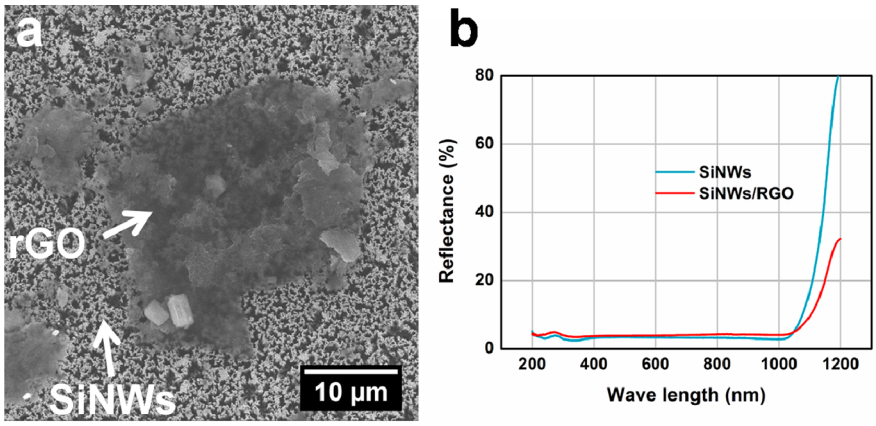

Figure 1. (a) Typical plane-view SEM image of the SiNWs/rGO sample and (b) reflectance spectra of SiNWs/rGO and SiNWs samples.

Hummers' method,[32] and the SiNWs/rGO composites were obtained via convenient spin-coating. The resulting SiNWs/rGO composite exhibits enhanced photoelectrochemical properties, with short-circuit photocurrent density more than 4 times higher than that of the pristine SiNWs and more than 600 times higher than that of the planar Si/rGO composite. In consideration of the excellent optical absorption capability of SiNWs and the abundant possibility in the chemical modification of graphene, the method and results shown here indicate a convenient and applicable approach for further exploitation of high activity materials for photoelectrochemical hydrogen production.

EXPERIMENTAL METHODS

Fabrication of Si Nanowires. Si substrate (p type, 100 oriented, 1−10 Ω cm) was degreased by ultrasonication in sequence in ethanol and acetone each for 15 min and then rinsed with copious amount of deionized water. Afterward, the degreased Si substrates were subjected to a boiling solution composed of H_2O_2, $NH_3{\cdot}H_2O$, and H_2O (1:1:5, v/v/v) for 30 min, following by deionized water rinsing. In a typical MACE process, the cleaned Si substrates were immersed in an aqueous etchant ($AgNO_3$, 20 mM; HF, 4.5 M) for 30 min at room temperature (~25 °C). Afterward, the silver dentrites covering SiNWs samples were removed by diluted HNO_3 immersion for 5 min. The SiNWs were rinsed with deionized water and finally dried at 80 °C in air.

Fabrication of rGO. Graphene oxide was fabricated by the method introduced in ref 32. In brief, a mixture of graphite flakes (0.3 g) and $KMnO_4$ (1.8 g) was added to 40 mL of a mixture of H_2SO_4/H_3PO_4 (9:1, v/v), and the resulting mixture was heated at 50 °C for 12 h. Afterward, the mixture was poured onto ice (40 mL) with 30% H_2O_2 (0.3 mL). The golden-yellow product (graphene oxide) was washed in succession with deionized water and diluted HCl and further purified by dialysis. To reduce graphene oxide, 0.1 g of graphene oxide was dispersed in 100 mL of deionized water by 30 min ultrasonication and reduced by 5 mL of hydrazine hydrate (85%) at 100 °C for 24 h. The resulting rGO was washed by repeated centrifugation/ultrasonication treatments.

Fabrication of SiNWs/rGO. The SiNWs/rGO composites were obtained by spin-coating. Prior to spin-coating, the mixture of rGO (8 mg) and ethanol (10 mL) was sonicated for 30 min. In a typical spin-coating process, 200 μL of rGO/ethanol dispersion was dropped onto the SiNWs sample, and the SiNWs sample was rotated at 600 rpm for 1 min and then at 4000 rpm for 5 min.

Morphology Characterization. The morphology of SiNWs/rGO was accessed by scanning electron microscopy (SEM, 7001F, JEOL).

Spectroscopy Characterization. Fourier transform-infrared (FT-IR) spectra of GO and rGO were recorded using a Thermo Nicolet NEXUS FT-IR spectrophotometer. Raman spectra of GO and rGO were measured on a Renishaw inVia Raman spectrometer. The reflectance spectra of SiNWs and SiNWs/rGO samples were measured on a UV−vis-near IR spectrophotometer (UV 4100, Hitachi).

Electrochemical Measurement. The photoelectrochemical measurements of SiNWs and SiNWs/rGO were carried out in aqueous H_2SO_4 solution containing 0.5 M K_2SO4 (pH = 1.8) with an electrochemical workstation (CHI 614D, CH Instrument). A three-electrode configuration was adopted in the measurements, with SiNWs or SiNWs/rGO as the working electrode, a Pt foil (1 × 1 cm^2) as the counter electrode, and a mercury/mercurous sulfate reference electrode (MSE) as the reference electrode. The reversible hydrogen evolution potential (RHE) was measured in the same solution using a clean Pt electrode as the working electrode and MSE as the reference electrode,[11,33] being −0.754 V vs MSE (Figure S1, Supporting Information). Therefore, a potential measured with respect to the MSE electrode was referenced to RHE by adding a value of 0.754 V. SiNWs samples were assembled into a homemade electrochemical cell, with only a defined area (0.07 cm^2) of the front surface of the sample exposed to the solution during measurements. An indium−gallium alloy (99.99%, Sigma-Aldrich) was applied to the back-side of SiNWs samples enabling ohmic contact. For photoelectrochemical measurement, the illumination was generated by a 300 W xenon lamp, and the incident light density was adjusted to 100 mW/cm^2 prior to each experiment. In a typical photoelectrochemical evaluation, a SiNWs sample was subjected to photocurrent density (J) versus potential (E) and impedance measurements. Afterward, the SiNWs sample was immersed in diluted HF aqueous solution (~5 wt %) for 5 min to remove possibly formed SiO_2, and then the sample was rinsed with a copious amount of deionized water. The cleaned SiNWs sample was then spin-coated with rGO, resulting in a SiNWs/rGO sample. Finally, the SiNWs/rGO sample was subjected to J−E and impedance measurements.

RESULTS AND DISCUSSION

The reduction of GO to rGO can be visualized by the color change of the product, in which the brownish reactant turns black (Figure S2, Supporting Information). The reduction of graphene oxide strips into rGO was further suggested by the FT-IR spectra (Figure S3, Supporting Information), which shows the obvious diminishing of absorptions at 1725 cm^{-1} (C═O stretching of COOH groups), 1635 cm^{-1} (O−H bending vibration of epoxide groups), and 1400 cm^{-1} (tertiary C−OH groups)[34,35] and Raman spectra (Figure S4, Supporting Information), which shows an increased D/G intensity ratio from rGO in comparison with GO.[36] The Si substrate subjected to the MACE process evolves to well-defined Si nanowires with ~4 μm length (Figure S5, Supporting Information). After the spin-coating, rGO is located on the top of SiNWs (Figure 1a). It is shown that the lateral sizes of the rGO strips vary from

dx.doi.org/10.1021/am3027458 | ACS Appl. Mater. Interfaces 2013, 5, 1961−1966

several micrometers to several tens of micrometers, and rGO strips are sufficiently thin to be semitransparent so that SiNWs below rGO strips can be observed in SEM. In addition, a low-magnification SEM image (Figure S6, Supporting Information) reveals that rGO strips cover ~2.5% of the surface area of the SiNWs sample. The reflectance performance of SiNWs/rGO is nearly identical to that of pristine SiNWs (Figure 1b), with the reflectance less than 4% within a wavelength interval of 200–1000 nm. The difference is that the SiNWs/rGO sample shows smaller reflectance than the SiNWs sample when the wavelength is larger than ~1000 nm. The improvement of absorption in the large wavelength range (~>1000 nm) can be attributed to the absorption of a photon by rGO.

The photoelectrochemical measurements were carried out in aqueous H_2SO_4 solution containing 0.5 M K_2SO_4 (pH = 1.8). The representative results are shown in Figure 2. Under illumination, Si nanowires exhibit larger current density (circle in Figure 2) in comparison with that measured in the dark (squares in Figure 2). When the SiNWs sample was spin-coated with rGO, the current density measured under illumination (downward triangles in Figure 2) is also larger than that measured in the dark (upward triangles in Figure 2). It is worth noting that the SiNWs/rGO sample exhibits remarkably larger photocurrent density, in comparison with the SiNWs sample. Continuous hydrogen bubbles can be found to evolve from the surface of the SiNWs/rGO sample during the measurement, and the current fluctuation around −0.4 V (vs RHE) for SiNWs/rGO sample can be attributed to hydrogen bubbles on the surface of the sample reducing the active area of sample or in the electrolyte scattering the incident illumination. The qualitative of illustration of such enhancement can be found in Figure S7 (Supporting Information), which shows that the photocurrent density of SiNWs/rGO sample is more than 4 times of that of SiNWs around 0 V (vs RHE) and near two times at −0.3~−0.1 V (vs RHE). Moreover, the photocurrent of SiNWs/rGO is also much larger than that of the planar Si/rGO sample (Figure S8a, Supporting Information), with an enhancement factor ranging 150–600 (Figure S8b, Supporting Information).

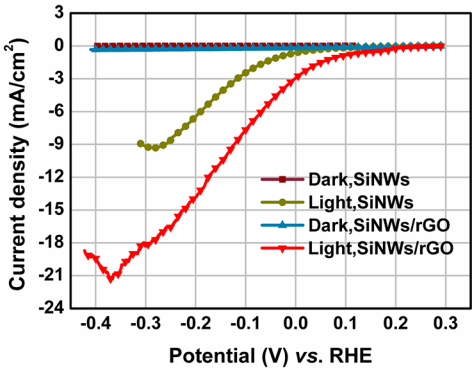

Figure 2. Photoelectrochemical behavior of SiNWs and SiNWs/rGO samples.

The short-circuit photocurrent density of SiNWs/rGO (J_{sc}), which is defined as the photocurrent density at 0 V (vs RHE),[11] is as large as 3.0 mA/cm^2. In addition, it can be revealed that the open circuit potential of the SiNWs/rGO sample (0.206 V vs RHE) is 20 mV positively shifted in comparison with that of the SiNWs sample (0.186 V vs RHE). On the other hand, the stability of SiNWs/rGO sample was evaluated by photocurrent density-time measurement, which shows that the photocurrent degradation is negligible after 10 min of constant illumination

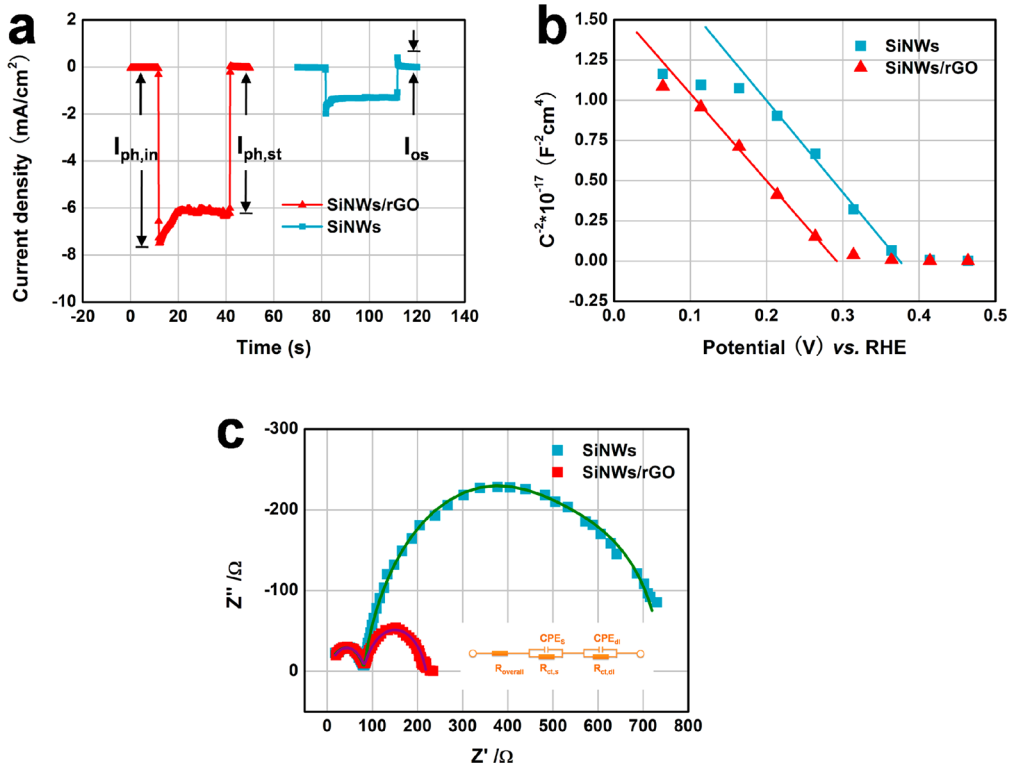

Figure 3. (a) Transient IV behaviors of SiNWs and SiNWs/rGO samples under chopped illumination at V_a = 0.09 V (vs RHE). (b) Mott–Schottky plot of SiNWs and SiNWs/rGO samples. (c) EIS spectra of SiNWs and SiNWs/rGO sample measured at V_a = −0.11 V (vs RHE).

dx.doi.org/10.1021/am3027458 | ACS Appl. Mater. Interfaces 2013, 5, 1961–1966

(Figure S9, Supporting Information). Three pairs of SiNWs/rGO and pristine SiNWs samples were subjected to the photocurrent measurements, and remarkably enhanced photocurrent can always be found in SiNWs/rGO samples, in comparison with the corresponding pristine SiNWs. These results show definitely that the addition of rGO to SiNWs samples can remarkably improve the photoelectrochemical properties.

Table S1 (Supporting Information) lists the photoelectrochemical photocurrent densities of SiNWs or Si microwires-based photocathode with different modification strategies in the photoelectrochemical hydrogen production. Although the J_{sc} of SiNWs/rGO remains lower than that of SiNWs or Si microwires functionalized with platinum particles and Mo_3S_4 cluster (as electrocatalyst), the J_{sc} of SiNWs/rGO is larger than those of SiNWs modified with MoS_2 (as electrocatalyst) and ZnO (for charge separation) and planar Si modified with rhenium or ZnO nanowires.

To find out possible factors inducing the enhanced performance, a variety of electrochemical experiments were carried out. First, the transient behaviors of the photocurrent of SiNWs and SiNWs/rGO under chopped illumination were monitored (Figure 3a). Similar behavior to that has been shown in Figure 2, and SiNWs/rGO exhibits a larger photocurrent density than SiNWs under the same applied potential. Moreover, the $I_{ph,st}/I_{ph,in}$ ratio of SiNWs sample (0.65) is smaller than that of SiNWs/rGO (0.82), where $I_{ph,st}$ is the stationary photocurrent density under illumination, and $I_{ph,in}$ is the initial photocurrent density spike just obtained at the moment the light is switched on. On the other hand, the I_{os} of SiNWs sample (0.41 mA/cm^2) is much larger than that of the SiNWs/rGO sample (0.04 mA/cm^2), where I_{os} is the spike of "overshoot" current density obtained at the moment the light is switched off. The smaller $I_{ph,st}/I_{ph,in}$ ratio and much larger I_{os} in the SiNWs sample suggests that more carriers are trapped and combined at the surface state of the SiNWs in the SiNWs sample, in comparison with those in the SiNWs/rGO sample.[37,38]

Different band bending of SiNWs in the SiNWs sample and SiNWs/rGO sample might be one possible factor reducing the charge trapping in the SiNWs/rGO sample. To verify this assumption, the flat band potential (V_{fb}) of SiNWs and SiNWs/rGO samples were determined. The flat band energy of SiNWs and SiNWs/rGO can be extracted from the capacitance versus applied potential relation via the Mott−Schottky relationship,[39] $1/C^2 = 2(V_a - V_{fb} - kT/q)/(qN_d\varepsilon_s\varepsilon_0A^2)$, where C is the space charge capacity, V_a is the applied potential, k is the Boltzmann constant, T is the absolute temperature, q is the electron charge, N_d is the donor density, ε_s is the dielectric constant of materials, ε_0 is the electric permittivity of vacuum, and A is area. The corresponding Mott−Schottky plot is shown in Figure 3b, giving the flat band potential of 0.28 V (vs RHE) for SiNWs/rGO and 0.36 V (vs RHE) for SiNWs.

The band bending (V_b) in the semiconductor is determined by the applied potential and the flat band potential according to the formula: $V_b = V_a - V_{fb}$. Because all of the applied potential are more negative than the flat band potential of the SiNWs and SiNWs/rGO samples, the more positive flat band potential of the SiNWs results in larger band bending than the SiNWs/rGO under identical applied potentials. The larger band bending separates the photogenerated electron−hole pairs faster, reducing the surface trapping and recombination of photogenerated carriers.[40] Therefore, from an energetics perspective the smaller band bending of SiNWs/rGO would contribute negatively to charge separatio, and cannot afford the different transient behaviors shown in Figure 3a and the enhancement performance shown in Figure 2.

Electrochemical impedance spectroscopy (EIS) has become a powerful tool to access the charge transfer property of charge transfer process in photoelectrochemical devices.[41,42] The EIS measurements were carried out at −0.11 V (vs RHE) under 100 mW/cm^2 illumination covering a frequency interval of 10^6−1 Hz. The typical results are presented in Figure 3c in the form of Nyquist plots, where the scatters (squares and triangles) are the experimental data and the solid lines are the results of fitting the experimental data to an equivalent circuit shown in the inset of Figure 3c (see also in Figure S10, Supporting Information). In typical three electrode experiments, the effect of the counter electrode is excluded. The two capacitance elements suggested by EIS spectra can be assigned to the capacitance of the depletion layer in the semiconductor and the capacitance of the double layer at the semiconductor−electrolyte interface.[43] In the equivalent circuit, $R_{overall}$ represents the overall series resistance, CPE_S is the capacitance phase element for the depletion layer of semiconductor, $R_{ct,S}$ is the charge transfer resistance in the depletion layer of the semiconductor, CPE_{dl} is the capacitance phase element for the double layer at the semiconductor−electrolyte interface, and $R_{ct,dl}$ is the charge transfer resistance of the double layer at the semiconductor−electrolyte interface. The $R_{ct,dl}$ is correlated to the kinetics of the faradaic reaction across the double layer (i.e., the reduction of H^+ to hydrogen in our experiments), with a smaller value corresponding to a faster reaction rate.[44]

The high frequency response in EIS can be attributed to the charge transfer process in the depletion layer of the semiconductor (i.e., SiNWs and SiNWs/rGO). The low-frequency response can be associated with charge transfer across the double layer at the semiconductor−electrolyte interface. The SiNWs/rGO sample shows a smaller semicircle in the low frequency range, implying a smaller $R_{ct,dl}$ in the SiNWs/rGO sample, in comparison with the SiNWs sample. The value of elements in the equivalent circuit (inset of Figure 3c) can be extracted from the experimental EIS spectra by the data fitting, and the results are listed in Table S2 (Supporting Information). The fitted value of $R_{ct,dl}$ is 646 and 137 Ω for SiNWs and SiNWs/rGO, respectively. The charge transfer resistance of the double layer in the SiNWs/rGO experiment is approximately 4 times smaller than that of the SiNWs experiment, showing a good correlation with the larger photocurrent density in the SiNWs/rGO sample (Figure 2).

The promotion of charge transfer across the double layer through the rGO−electrolyte interface and consequently reduction of H^+ into H_2 can be further confirmed by comparative experiments. In the experiments, the J−E curves of bare fluorine doped tin oxide (FTO) and rGO-coated FTO were measured in the dark and with illumination. It is shown that the J−E curve of both samples are superposed by the corresponding dark current (Figure S11a, Supporting Information), confirming that rGO itself does not exhibit the photoresponse behavior. Moreover, the current of rGO-coated FTO sample is obviously larger than that of FTO under the same applied bias (Figure S11a, Supporting Information), confirming that rGO can accelerate the charge transfer across the double layer and the reduction of H^+. In addition, comparative experiments were conducted on glass carbon electrode (GC) loaded with and without rGO, and the

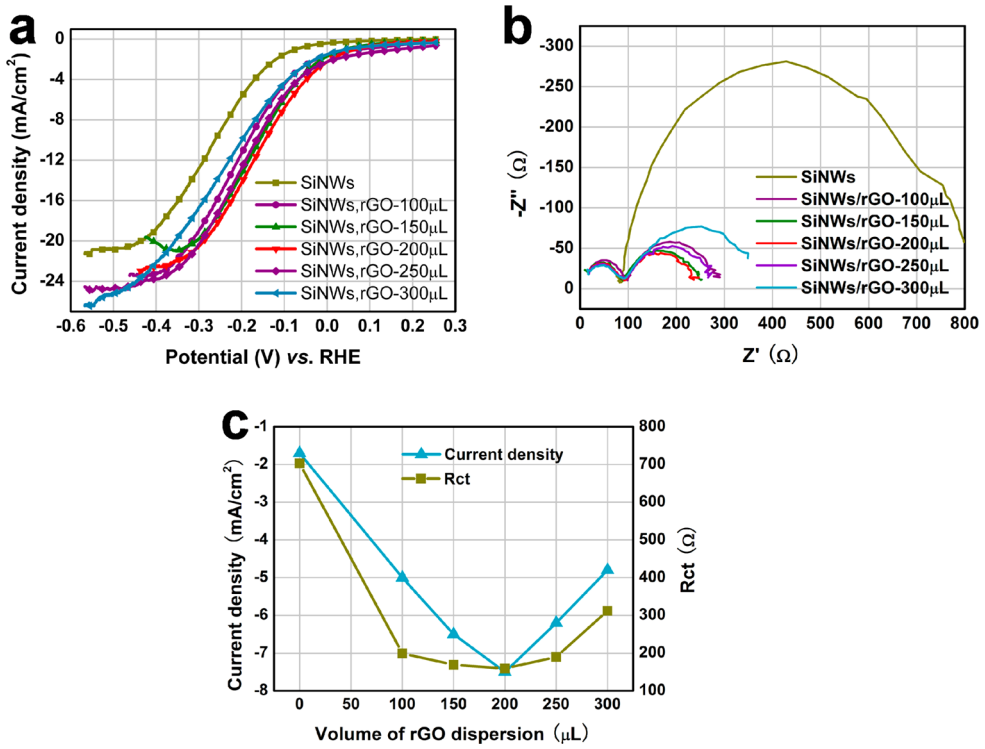

Figure 4. (a) Photocurrent density−voltage curve of SiNWs and SiNWs/rGO samples coated with different amounts of rGO measured with illumination. (b) EIS spectra of SiNWs and SiNWs/rGO samples coated with a different total amount of rGO. (c) Variation of $R_{ct,dl}$ and photocurrent density at −0.11 V (vs RHE) with the amount of rGO.

enhanced current from GC/rGO can be found (Figure S11b, Supporting Information), suggesting that the fast electron transfer is caused by the unique structure of rGO. Therefore, the enhance performance of SiNWs/rGO samples can be attributed to a kinetics effect, in which rGO acts as a channel for fast charge transfer from SiNWs to rGO and from rGO to electrolyte, reducing the trapping and recombination of photogenerated carriers and accelerating the reduction of H^+ in the electrolyte into hydrogen.

The influence of the coating amount of rGO on SiNWs was also investigated. In this experiment, the same SiNWs sample was subjected five times to rGO spin coating, and the photovoltaic performance was measured after each coating procedure. The resulting *J*−*E* curves (Figure 4a) show that the photocurrent densities of all rGO coated samples are larger than that of a pristine SiNWs sample and that the optimal performance are achieved when the total added volume of rGO dispersion was increased to 200 μL. The EIS measurements were also carried out after each photocurrent measurements under −0.11 V (vs RHE) and 100 mW/cm^2 illumination. The Nyquist plots of the EIS spectra are presented in Figure 4b, showing that the pristine SiNWs sample and SiNWs sample totally spin-coated with 200 μL of rGO dispersion possess the largest and smallest semicircle in the intermediate frequency range, respectively. The photocurrent densities of the pristine SiNWs sample and SiNWs samples spin-coated with a different total volume of rGO dispersion are listed in Figure 4c, accompanied with the charge transfer resistance of the double layer of each sample extracted from the corresponding EIS spectra by fitting the experimental data to the equivalent circuit (inset of Figure 3c). It is shown that the photocurrent density at this applied potential can be well correlated with the charge transfer resistance of each sample.

In the above discussion, it has been proposed that the contact between SiNWs and rGO offers a channel for the fast electron transfer from SiNWs to rGO and then from rGO to the electrolyte. Therefore, increasing the amount of spin-coated rGO will increase the amount of such channels (SiNWs-rGO-electrolyte), improving the performance of the samples. However, when the amount of rGO is further increased, the latter coated rGO strips would possibly be located on the former coated rGO strips. It means that the thickness and accordingly the series resistances of some rGO strips would be increased. If their series resistance is sufficiently large, such rGO strips will no longer act as channels for fast electrons transfer, and the amount of active channels for fast electrons will be reduced. It can therefore be found in experiments that the total charge transfer resistance of samples first increases and then decreases with the amount of rGO dispersion (Figure 4c).

CONCLUSIONS

In summary, SiNWs/rGO composites were fabricated via a low-cost and convenient method. The SiNWs/rGO composite exhibits significantly improved photoelectrochemical properties, in comparison with the pristine SiNWs and planar Si/rGO samples. The influence of the addition amount of rGO to SiNWs on the photoelectrochemical properties was evaluated. The enhancement was tentatively ascribed to the positive contribution of rGO on the charge separation process in SiNWs and the charge transfer process at the rGO−electrolyte interface. The method and results presented here afford the further exploration of solar water-splitting materials with practical application and commercial benefits.

dx.doi.org/10.1021/am3027458 | ACS Appl. Mater. Interfaces 2013, 5, 1961−1966

■ ASSOCIATED CONTENT

Supporting Information

Determination of RHE, photograph of GO and rGO, FT-IR and Raman spectra of GO and rGO, cross-sectional view SEM image of SiNWs, low-magnification plan-view SEM image of SiNWs/rGO composite, enhancement of the photocurrent of SiNWs/rGO in comparison with SiNWs, the dark current and photocurrent of planar Si and planar Si/rGO, enhancement of the photocurrent of SiNWs/rGO in comparison with planar Si/rGO, the photocurrent density−time relation of SiNWs/rGO sample, the reported J_{sc} (photocurrent density at RHE) of photoelectrochemical hydrogen production of SiNWs or Si microwire based composites, equivalent circuit of SiNWs and SiNWs/rGO, the fitting results of EIS spectra shown in Figure 3c using the equivalent circuit in its inset, and the $J-V$ curves of FTO and FTO/rGO measured in the dark and under illumination. This material is available free of charge via the Internet at http://pubs.acs.org.

■ AUTHOR INFORMATION

Corresponding Author

*Zhipeng Huang: e-mail, zphuang@ujs.edu.cn. Chi Zhang: e-mail, chizhang@ujs.edu.cn; fax, 86-511-8879-7815.

Notes

The authors declare no competing financial interest.

■ ACKNOWLEDGMENTS

This research was financially supported by the National Natural Science Foundation of China (Grants 61006049, 61274105, 50925207), the Ministry of Science and Technology of China (Grant 2009DFA50620), the Ministry of Education of China (Grant IRT1064), the Education Department of Jiangsu (Grant 10KJB430004), and Jiangsu University (Grant 09JDG043 and Outstanding Youth Project), and Shanghai Municipal Education Commission Grant No. 06ZZ31.

■ REFERENCES

(1) Kayes, B. M.; Atwater, H. A.; Lewis, N. S. *J. Appl. Phys.* **2005**, *97*, 114302.
(2) Bookbinder, D. C.; Bruce, J. A.; Dominey, R. N.; Lewis, N. S.; Wright, M. S. *Proc. Natl. Acad. Sci. U.S.A.* **1980**, *77*, 6280−6284.
(3) Szklarczyk, M.; Bockris, J. O. M. *J. Phys. Chem.* **1984**, *88*, 1808−1815.
(4) Peng, K. Q.; Wang, X.; Wu, X. L.; Lee, S. T. *Nano Lett.* **2009**, *9*, 3704−3709.
(5) Boettcher, S. W.; Spurgeon, J. M.; Putnam, M. C.; Warren, E. L.; Turner-Evans, D.; Kelzenberg, M. D.; Maiolo, J. R.; Atwater, H. A.; Lewis, N. S. *Science* **2010**, *327*, 185−187.
(6) Hou, Y. D.; Abrams, B. L.; Vesborg, P. C. K.; Bjorketun, M. E.; Herbst, K.; Bech, L.; Setti, A. M.; Damsgaard, C. D.; Pedersen, T.; Hansen, O.; Rossmeisl, J.; Dahl, S.; Norskov, J. K.; Chorkendorff, I. *Nat. Mater.* **2011**, *10*, 434−438.
(7) Peng, K. Q.; Lee, S. T. *Adv. Mater.* **2011**, *23*, 198−215.
(8) Wang, X.; Peng, K. Q.; Pan, X. J.; Chen, X.; Yang, Y.; Li, L.; Meng, X. M.; Zhang, W. J.; Lee, S. T. *Angew. Chem., Int. Ed.* **2011**, *50*, 9861−9865.
(9) Dominey, R. N.; Lewis, N. S.; Bruce, J. A.; Bookbinder, D. C.; Wrighton, M. S. *J. Am. Chem. Soc.* **1982**, *104*, 476.
(10) Szklarczyk, M.; Bockris, J. O. M. *Appl. Phys. Lett.* **1983**, *42*, 1035.
(11) Boettcher, S. W.; Warren, E. L.; Putnam, M. C.; Santori, E. A.; Turner-Evans, D.; Kelzenberg, M. D.; Walter, M. G.; McKone, J. R.; Brunschwig, B. S.; Atwater, H. A.; Lewis, N. S. *J. Am. Chem. Soc.* **2011**, *133*, 1216−1219.
(12) Oh, I.; Key, J. H.; Hwang, S. P. *Nano Lett.* **2012**, *12*, 298−302.
(13) Warren, E. L.; McKone, J. R.; Atwater, H. A.; Gray, H. B.; Lewis, N. S. *Energy Environ. Sci.* **2012**, *5*, 9653−9661.
(14) Tran, P. D.; Pramana, S. S.; Kale, V. S.; Nguyen, M.; Chiam, S. Y.; Batabyal, S. K.; Wong, L. H.; Barber, J.; Loo, J. *Chem.—Eur. J.* **2012**, *18*, 13994−13999.
(15) Sun, K.; Jing, Y.; Li, C.; Zhang, X.; Aguinaldo, R.; Kargar, A.; Madsen, K.; Banu, K.; Zhou, Y. C.; Bando, Y.; Liu, Z.; Wang, D. *Nanoscale* **2012**, *4*, 1515−1521.
(16) Novoselov, K. S.; Geim, A. K.; Morozov, S. V.; Jiang, D.; Zhang, Y.; Dubonos, S. V.; Grigorieva, I. V.; Firsov, A. A. *Science* **2004**, *306*, 666.
(17) Allen, M. J.; Tung, V. C.; Kaner, R. B. *Chem. Rev.* **2010**, *110*, 132−145.
(18) Xiang, Q. J.; Yu, J. G. *Chem. Soc. Rev.* **2012**, *41*, 782−796.
(19) Zhang, X. Y.; Li, H. P.; Cui, X. L.; Lin, Y. H. *J. Mater. Chem.* **2010**, *20*, 2801−2806.
(20) Li, Q.; Guo, B. D.; Yu, J. G.; Ran, J. R.; Zhang, B. H.; Yan, H. J.; Guo, J. R. *J. Am. Chem. Soc.* **2011**, *133*, 10878−10884.
(21) Zhang, J.; Yu, J. G.; Jaroniec, M.; Gong, J. R. *Nano Lett.* **2012**, *12*, 4584−4589.
(22) Ng, Y. H.; Iwase, A.; Kudo, A.; Amal, R. *J. Phys. Chem. Lett.* **2010**, *1*, 2607−2612.
(23) Chen, C. C.; Aykol, M.; Chang, C. C.; Levi, A. F. J.; Cronin, S. B. *Nano Lett.* **2011**, *11*, 1863−1867.
(24) Adhikari, S.; Ghimire, D. C.; Adhikary, S.; Uchida, H.; Wakita, K.; Umeno, M. *2012 38th IEEE Photovoltaic Spec. Conf. (Pvsc)* **2012**, 2500−2503.
(25) Li, X. M.; Zhu, H. W.; Wang, K. L.; Cao, A. Y.; Wei, J. Q.; Li, C. Y.; Jia, Y.; Li, Z.; Li, X.; Wu, D. H. *Adv. Mater.* **2010**, *22*, 2743−+.
(26) Feng, T. T.; Xie, D.; Lin, Y. X.; Zang, Y. Y.; Ren, T. L.; Song, R.; Zhao, H. M.; Tian, H.; Li, X.; Zhu, H. W.; Liu, L. T. *Appl. Phys. Lett.* **2011**, *99*, 233505.
(27) Lee, J. K.; Smith, K. B.; Hayner, C. M.; Kung, H. H. *Chem. Commun.* **2010**, *46*, 2025−2027.
(28) Wang, J. Z.; Zhong, C.; Chou, S. L.; Liu, H. K. *Electrochem. Commun.* **2010**, *12*, 1467−1470.
(29) Wang, X. L.; Han, W. Q. *ACS Appl. Mater. Interfaces* **2010**, *2*, 3709−3713.
(30) Lu, Z. Y.; Zhu, J. X.; Sim, D.; Shi, W. H.; Tay, Y. Y.; Ma, J.; Hng, H. H.; Yan, Q. Y. *Electrochim. Acta* **2012**, *74*, 176−181.
(31) Huang, Z. P.; Geyer, N.; Werner, P.; de Boor, J.; Gosele, U. *Adv. Mater.* **2011**, *23*, 285−308.
(32) Marcano, D. C.; Kosynkin, D. V.; Berlin, J. M.; Sinitskii, A.; Sun, Z. Z.; Slesarev, A.; Alemany, L. B.; Lu, W.; Tour, J. M. *ACS Nano* **2010**, *4*, 4806−4814.
(33) Walter, M. G.; Warren, E. L.; McKone, J. R.; Boettcher, S. W.; Mi, Q. X.; Santori, E. A.; Lewis, N. S. *Chem. Rev.* **2010**, *110*, 6446−6473.
(34) Nethravathi, G.; Rajamathi, M. *Carbon* **2008**, *46*, 1994−1998.
(35) Hou, C. Y.; Zhang, Q. H.; Zhu, M. F.; Li, Y. G.; Wang, H. Z. *Carbon* **2011**, *49*, 47−53.
(36) Stankovich, S.; Dikin, D. A.; Piner, R. D.; Kohlhaas, K. A.; Kleinhammes, A.; Jia, Y.; Wu, Y.; Nguyen, S. T.; Ruoff, R. S. *Carbon* **2007**, *45*, 1558−1565.
(37) Salvador, P. *J. Appl. Phys.* **1984**, *55*, 2977.
(38) Peter, L. M. *Chem. Rev.* **1990**, *90*, 753−769.
(39) Barsoukov, E.; Macdonald, J. R., *Impedance Spectroscopy Theory, Experiment, and Applications*; Wiley: New York, 2005.
(40) Michalak, D. J.; Gstrein, F.; Lewis, N. S. *J. Phys. Chem. C* **2008**, *112*, 5911−5921.
(41) Wang, Q.; Moser, J. E.; Gratzel, M. *J. Phys. Chem. B* **2005**, *109*, 14945−14953.
(42) Li, H. X.; Cheng, C. W.; Li, X. L.; Liu, J. P.; Guan, C.; Tay, Y. Y.; Fan, H. J. *J. Phys. Chem. C* **2012**, *116*, 3902−3807.
(43) Lopes, T.; Andrade, L.; Ribeiro, H. A.; Mendes, A. *Int. J. Hydrogen Energy* **2010**, *35*, 11601−11608.
(44) Merki, D.; Vrubel, H.; Rovelli, L.; Fierro, S.; Hu, X. L. *Chem. Sci.* **2012**, *3*, 2515−2525.